Dyrobes®
Dyrobes Rotordynamics Software
http://dyrobes.com

Bump Foil Damping Using a Simplified Model

Erik E. Swanson
Xdot Engineering and Analysis,
112 Woodbridge Lane,
Chapel Hill, NC 27514
e-mail: Erik@XdotEA.com

Foil bearings are a key enabling technology for advanced and oil-free rotating machinery. In certain applications, they provide a level of performance that is difficult or impossible to match with other technologies. A number of reasonably successful analytical techniques to predict bearing load capacity, power loss, and stiffness have been developed. Prediction of damping, however, has remained problematic. This work presents a fresh look at the damping problem. Using a simplified representation of a bump foil, this work considers explicitly adding the load dependence of the friction force. This approach is shown to provide a good match to previous experimental data. Parametric study results for the various model parameters are presented to examine the characteristics of this model. It is concluded that the load-dependent frictional force is important to consider for a bump foil damping model. [DOI: 10.1115/1.2197838]

Keywords: damping, foil bearing, friction, multi-harmonic balance

Introduction

Since the first foil bearing paper was published 1953 by Blok and Van Rossum [1], considerable progress has been made in the design and application of these bearings. They have long been a standard bearing choice for air cycle machines used for aircraft cabin pressurization [2] and are being used by at least one commercial manufacturer of small microturbines [3]. Other applications proposed or developed range from turbo-expanders and cryocoolers, to turbochargers [4]. An industrial plant air compressor operating above a bending critical speed has also been demonstrated and was reported to be in beta testing [5]. With advancements in load capacity, temperature capability, and damping, some are seriously advocating the use of these bearings in aircraft gas turbines [6]. Thus, it is clear that foil bearings are a viable technology and can be successfully applied, at least for smaller machinery.

Analytical methods to predict foil bearing performance parameters have also been under development. Early work includes efforts by Oh and Rohde for multi-leaf designs [7] and efforts by Walowit et al. for the bump foil bearing [8]. More recent work includes a number of papers by Ku and Heshmat [9–12], Heshmat et al., [13], Peng and Carpino [14–16], Carpino and Talmage [17], Iordanoff et al. [18–20], Peng and Khonsari [21,22], San Andres [23], and Kim and San Andres [24]. From this body of work, and related experimental works, it seems that predictions of basic operating parameters (load capacity, power loss, stiffness) can be made with reasonable accuracy. Damping predictions have generally been more problematic. The analytical works vary somewhat in their approach to the problem. One approach is the assumption of a stiffness in parallel with an equivalent viscous damper calculated from the standard Coulomb friction equation. Complex/hysteretic damping as well as more complex energy-based approaches considering actual bump loading and motion are also suggested. Some of these seem complex to integrate with the dynamic model for the gas film.

In addition to the analytical developments, there have been several attempts to experimentally measure bump characteristics. These include static loading response, dynamic stiffness, and equivalent damping for a flat bump strip [11,25], as well as for partial or full bearing assemblies [26–32]. These studies generally support the idea that foil damping must be Coulomb-like, in that the damping estimates decay with frequency, and change with amplitude and load in roughly as would be expected from the standard equivalent damping equation for Coulomb friction. However, there are some discrepancies which suggest the Coulomb model does not capture all of the important features of the bump foil physics.

In evaluating the various models of bump foil behavior, it seems that desirable features for a model include

1. prediction of finite response amplitudes when excited at resonance,
2. prediction of the bounded subsynchronous limit cycle frequently observed when operating a foil bearing supported rotor above a rotor-bearing system natural frequencies, and providing a means of estimating the limit cycle amplitudes
3. providing a means of model parameter estimation from readily measurable characteristics, and
4. predicting behavior that is in reasonable agreement with the experimental data.

Coulomb Friction in Parallel With Spring

The simplest candidate model combines a simple Coulomb friction with equal static and dynamic coefficients of friction, as in Eq. (1), with a parallel spring as shown in Fig. 1. This model has been proposed as part of several foil bearing dynamic models.

$$F_d = \begin{cases} -\mu F0\, sign(\dot{x}) & \dot{x} \neq 0 \\ -\mu F0 < F_d < \mu F0 & \dot{x} = 0 \end{cases} \quad (1)$$

To evaluate this model under static loading, the static load deflection may be compared to the load deflection presented as "Left Pivot" in Fig. 6(a) of one of the Ku and Heshmat works [25]. This comparison is shown in Fig. 2. For the purposes of comparison, an offset has been added to the model to improve the agreement of higher loads during the initial loading portion of the cycle. The inclusion of an offset seems like a reasonable approximation to address the loss of contact at low load for several of the bumps on the six bump strip, as noted by the authors in the discussion of the experimental data. As shown in the figure, it is clear, though, that a simple Coulomb model does not agree very well with experimental data.

The first difference is that the Coulomb model has the same slope (stiffness) for loading and unloading, whereas the experimental data show a higher slope (stiffness) for loading than unloading. The second difference is the initial unloading behavior. The simple Coulomb model exhibits a constant displacement dur-

Contributed by the Tribology Division of ASME for publication in the JOURNAL OF TRIBOLOGY. Manuscript received August 29, 2005; final manuscript received March 1, 2006. Review conducted by Michael M. Khonsari.

 Copyright © 2006 by ASME

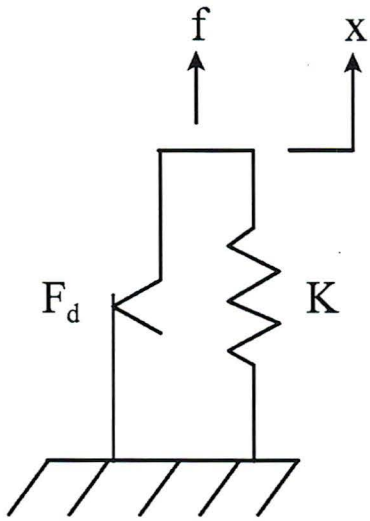

Fig. 1 Coulomb friction damper

ing initial unloading, whereas the experimental data show a decreasing displacement. The other difference is the behavior at low loads. The Coulomb model has a large force offset between loading and unloading at no load. The experimental data show a return to roughly the same zero location once load is removed.

To calculate equivalent dynamic characteristics, the friction element is frequently decoupled from the stiffness element and reduced to an equivalent viscous damping. Considering the energy dissipation, the equivalent damping for a Coulomb friction element is given by [33]:

$$C_{eq} = \frac{4F_d}{\pi\omega X} \tag{2}$$

where F_d is the constant friction force, ω is the excitation frequency, and X is the response amplitude. It can be shown that as soon as the applied force is large enough to overcome the friction and start to move, the amplitude at resonance is unbounded [33].

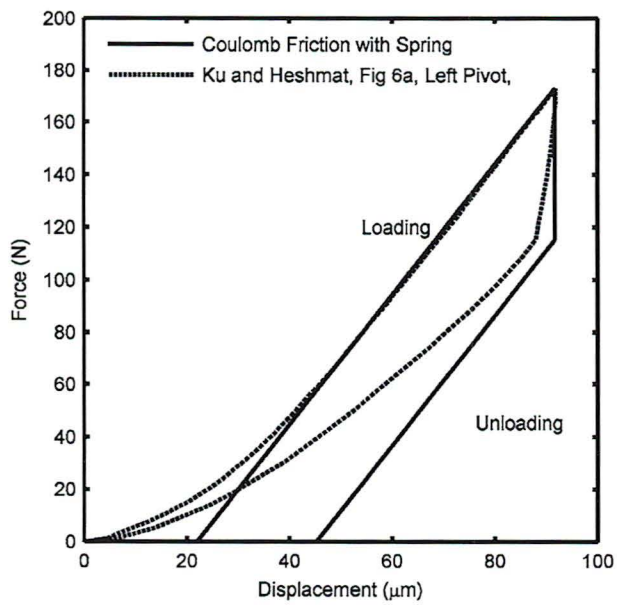

Fig. 2 Coulomb friction with spring versus Fig. 6(a), Left Pivot from [25]

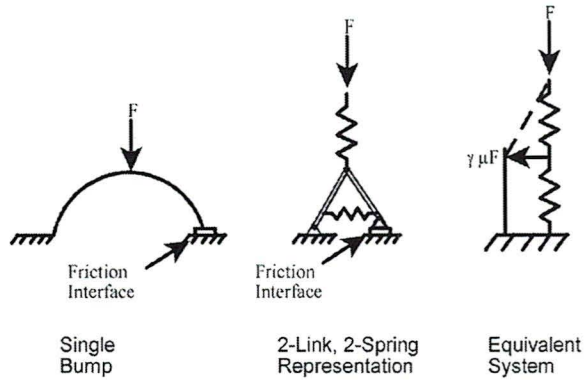

Fig. 3 Development of simplified bump model

Hence, the assumption of a standard simple Coulomb friction model violates the observed foil bearing behavior of an adequately damped response going through the lower rigid rotor modes and the usual claim of significantly higher damping than a rigid pad bearing under similar conditions.

Full Bump Model

A much more complex model is suggested by Walowit [8], with later extensions by Ku and Heshmat [9,26,12]. In these works, a fuller accounting is made of the physics, which include interactions between applied load, friction forces, multiple bumps on a single bump strip, as well as the stiffness of an individual bump. This model obtains much better agreement with the static load data. Unfortunately, the approach developed is more difficult to apply than simple Coulomb friction. The only approach suggested for estimating equivalent damping is via simulation and dissipated energy. Due to the relatively large number of parameters, it is also more difficult to use this model to obtain a basic understanding of the fundamental characteristics of bump damping.

Simplified Bump Model

In an attempt to develop a simpler model which could offer greater insight into the fundamental issues of bump foil damping, various approaches to simplification of the multi-bump, multi-friction interface were considered. The most successful approach was to focus on a single bump, with friction limited to a single interface. As will be seen, these two simplifications do not seem to adversely impact the general behavior of the model. This approach provides a very good approximation to experimentally noted behavior, yet remains fairly simple. The remainder of this paper focuses on the development of this model and the exploration of its characteristics.

From the perspective of a single bump, it is possible to progress to a fairly simple model when a single friction interface is assumed. This progression is illustrated in Fig. 3. It begins by replacing the distributed stiffness of a bump with two springs and a pair of rigid links. This system can be reorganized and simplified as shown in the final two-springs plus load-dependent friction element system. The load-dependent friction element is assumed to generate a force proportional to the applied load multiplied by a friction coefficient. In the model, it is represented as a coupling coefficient (γ) multiplied by a friction coefficient (μ). This system is similar to a two spring system with Coulomb friction, but with the important difference that the friction force is a function of the total applied load.

The use of a load-dependent friction force is similar to that reported for a beam with friction on a double-sided ramp reported by Whiteman and Ferri [34]. They found that adding a displacement/load dependence was beneficial with regards to controlling vibration amplitudes. Menq et al. [35] discuss using a

load-dependent friction force in a simple system. Using a two term harmonic balance, this work reports results that indicate the coupling coefficient plays an important role in the overall response.

In developing the system equations for the simple bump model, it will be assumed that the load-dependent friction element responds with a sliding force proportional to the applied load (linearly load-dependent Coulomb friction). For simplicity, it will also be assumed that the static coefficient of friction is equal to the sliding coefficient of friction. However, the model can be readily extended to a more complex model, such as that advocated by Lampaert et al. [36–38], which can include considerations of presliding hysteresis, a Stribeck curve for high velocities, friction lag, etc.

Adding a mass to the free end of the spring, assigning parameters, and labeling the degrees of freedom as shown in Fig. 4, a nonlinear set of system equations can be obtained for positive displacements (negative displacements are assumed to result in lift-off, and therefore no force generation) as shown in Eq. (3):

$$M\ddot{x}_1 + K_1(x_1 - x_2) = f \tag{3}$$

$$x_2 = \begin{cases} x_1 \dfrac{K_1(1-\gamma\mu)}{K_2 + K_1(1-\gamma\mu)} \text{ if } \dot{x}_1 > 0 \text{ and } x_1 > x_2 \dfrac{K_2 + K_1(1-\gamma\mu)}{K_1(1-\gamma\mu)} \\ x_1 \dfrac{K_1(1+\gamma\mu)}{K_2 + K_1(1+\gamma\mu)} \text{ if } \dot{x}_1 < 0 \text{ and } x_1 < x_2 \dfrac{K_2 + K_1(1+\gamma\mu)}{K_1(1+\gamma\mu)} \\ \dot{x}_2 = 0 \text{ otherwise} \end{cases}$$

One nice feature of these equations is that the simple bump model response does not depend on velocity or acceleration. Thus, the response of the friction element to displacement forcing at x_1 can be calculated very rapidly and easily by a simple difference equation as shown in Eq. (4). In this difference equation formulation, i is the current step and $i-1$ is the previous step. Note that the sliding conditions in the difference equation are the same as above, but reorganized slightly.

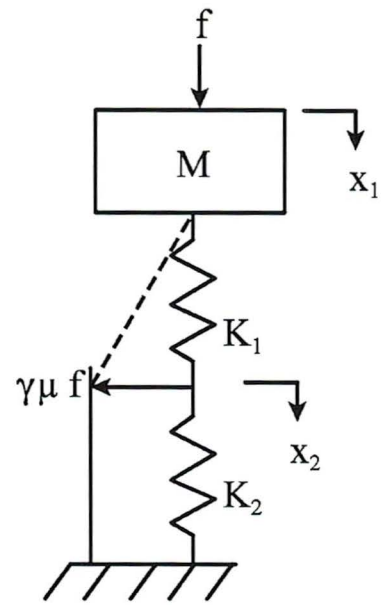

Fig. 4 Simple bump model with mass

$$x_{1_i} = \text{input}$$

$$x_{2_i} = \begin{cases} x_{1_i} \dfrac{K_1(1-\gamma\mu)}{K_2 + K_1(1-\gamma\mu)} & \text{if } x_{1_i} > x_{1_{i-1}} \text{ and } K_1(x_{1_i} - x_{2_{i-1}}) > [K_2 x_{2_{i-1}} + \gamma\mu(x_{1_i} - x_{2_{i-1}})] \\ x_{1_i} \dfrac{K_1(1+\gamma\mu)}{K_2 + K_1(1+\gamma\mu)} & \text{if } x_{1_i} < x_{1_{i-1}} \text{ and } K_1(x_{1_i} - x_{2_{i-1}}) < [K_2 x_{2_{i-1}} - \gamma\mu(x_{1_i} - x_{2_{i-1}})] \\ x_{2_{i-1}} & \text{otherwise} \end{cases} \tag{4}$$

Static Response

As a first test of the simple bump model, a comparison will be made to the load deflection presented previously. After adjusting the parameters to provide roughly the correct peak load/displacement point and unloading transition point, the comparison is as shown in Fig. 5. As with the Coulomb response, a displacement offset has again been added to the model response. This figure shows surprisingly good agreement between the simple three parameter model and the six bump strip loaded via a pivoted plate, especially at higher loads once all bumps are active.

One interesting feature of the model is that it predicts that the slope of the loading curve (and hence stiffness) is greater than the unloading curve. It also predicts a transition region during the initial unloading which has a much greater slope (and hence stiffness) than during loading or unloading. These two characteristics match the experimental data trends. The constant stiffnesses during loading and unloading are also interesting. They are due to the linear load dependence of the friction force. The difference between loading and unloading stiffness is due to the interaction between spring K_2 and the load-dependent friction element, which is also responsible for the high stiffness during the transition between loading and unloading.

Dynamic Response—Approach

With the model static response anchored to experimental results for a flat bump strip, the dynamic response will be considered. To evaluate the response, the nonlinear dynamic model can be integrated using Runge-Kutta, etc. However, this process takes a considerable length of time, particularly to perform a frequency sweep for several different cases, nor is this approach well suited to inclusion in an overall foil bearing analysis code, which really needs equivalent linear characteristics to include in the prediction of rotor dynamic coefficients.

One solution to this problem is to make use of the multiple harmonic balance (MHB) approach [39,40]. Briefly, this approach can be summarized as follows. Starting with the equations of motion for the mass-nonlinear element system written in the form of Eq. (5), the excitation and response are assumed to be periodic

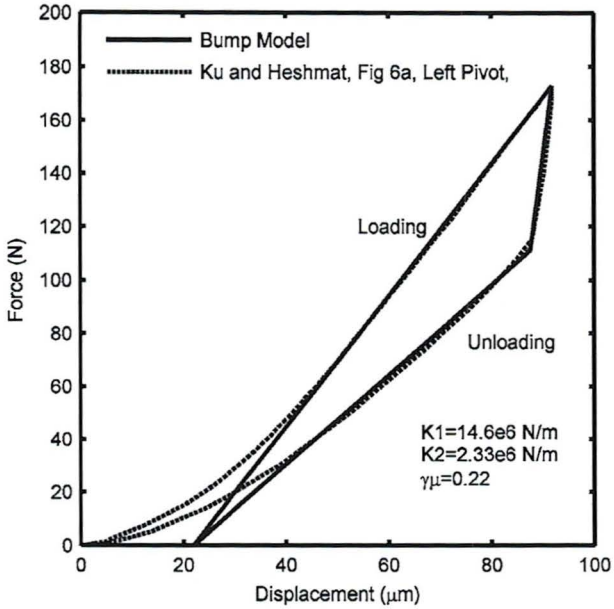

Fig. 5 Simplified bump model versus Fig. 6(a), Left Pivot from [25]

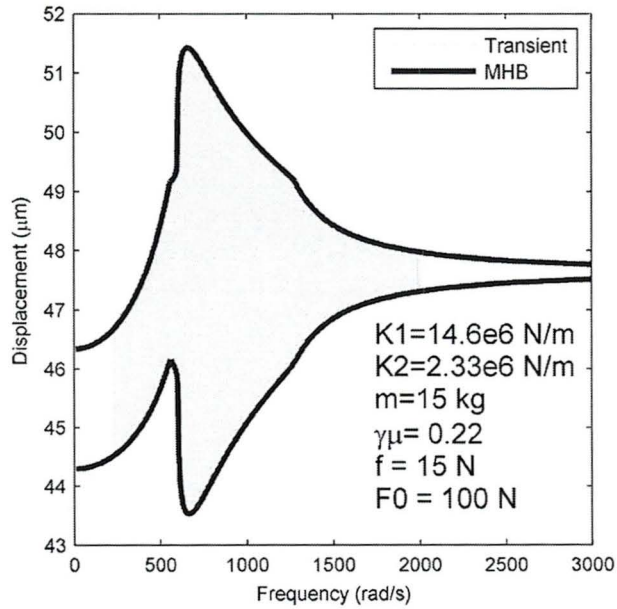

Fig. 6 Time transient and MHB responses

and are represented by a set of truncated Fourier series with matching fundamental frequencies as shown in Eqs. (6) and (7):

$$m\ddot{x}(t) + g(x(t)) - f(t) = 0$$

where

$$g(x(t)) = K_1[x_1(t) - x_2(t)] \tag{5}$$

$$x(t) = X0 + \sum_{k=1}^{n} [X_k^c \cos(k\omega t) + X_k^s \sin(k\omega t)] \tag{6}$$

$$f(t) = F0 + \sum_{k=1}^{n} [F_k^c \cos(k\omega t) + F_k^s \sin(k\omega t)] \tag{7}$$

where $g(x(t))$ is the nonlinear force from the simple bump model, and the other variables are as defined previously. The nonlinear function $g(x(t))$ is calculated as the load generated in spring K_1. For the purposes of this work, a single frequency excitation plus static load was assumed. The response includes a static offset, the fundamental and multiple harmonics. Using the frequency domain coefficients, an equation for the error between the applied force and the force corresponding to the assumed displacement can be written as in Eq. (8),

$$\mathbf{R} = \mathbf{Z} + \mathbf{G} - \mathbf{F} \tag{8}$$

where $a\mathbf{G} = (\mathbf{G}0, \mathbf{G}_1^c, \mathbf{G}_1^s, \ldots, \mathbf{G}_n^s)^T$ and $\mathbf{F} = (\mathbf{F}0, \mathbf{F}_1^c, \mathbf{F}_1^s, \ldots, \mathbf{F}_n^s)^T$ are the vectors of frequency domain components of the nonlinear bump force and the applied force, respectively, and $\mathbf{Z}$ is a diagonal matrix of inertia forces given by Eq. (9).

$$\mathbf{Z} = \begin{bmatrix} 0 & 0 & 0 & \ldots & & \\ 0 & -\omega^2 m & 0 & \ldots & & [0] \\ 0 & 0 & -\omega^2 m & \ldots & & \\ \ldots & \ldots & \ldots & \ldots & & \\ & & & & -n^2\omega^2 m & 0 \\ & [0] & & & 0 & -n^2\omega^2 m \end{bmatrix} \tag{9}$$

The residual equation was solved as a set of nonlinear equations using a trust-region dogleg method with finite differences to approximate the Jacobian [41]. For the first point of a set of solutions, the initial guess was the static displacement, with very small sin and cos components at the fundamental frequency, and zero for higher harmonics. For subsequent points, the previous point's solution was used as the initial guess. Some convergence difficulties were encountered when passing through resonance. It was found that using a new initial guess based on switching the synchronous cosine and sine components when problems were encountered near resonance generally resulted in convergence.

As noted in [39], once a set of displacement harmonics is specified, the calculations can be done more efficiently by using a fast fourier transform (FFT) and inverse fast fourier transform (IFFT). For this work, an IFFT is used to generate a 256 point (for one fundamental period) displacement time waveform. Two cycles of this waveform are then used as input to the difference equation for the nonlinear bump motion, to rapidly generate a time waveform for the bump force. A forward FFT is then performed on the second cycle of the resulting force waveform to calculate the set of frequency domain force coefficients for the nonlinear bump element. The use of only one cycle as a "settling" cycle was found to be sufficient in the cases examined. The second and subsequent cycles matched within a reasonable tolerance.

Comparison of MHB to Time Integration

As a first step, the frequency response of the simple bump model to a slow sine sweep will be presented. Using the set of bump parameters estimated from [25], and a mass of 15 kg, the response to a 10 N excitation with a 100 N static load is presented in Fig. 6. The shaded region is the time transient response to a slow sine sweep (if the shaded region were magnified, it would be seen as a set of very closely spaced sines of slowly increasing frequency). The solid black line is the MHB estimate of the response with the static offset and four harmonics. As can be seen, the MHB agrees quite well with the time transient. The results were examined for both increasing and decreasing excitation frequencies. For the parameter set specified, no difference was noted.

An important feature of this plot is the generally well-damped response passing through the region of the apparent natural frequency. The ability of the simplified bump model with load-dependent friction to pass through a resonance with finite ampli-

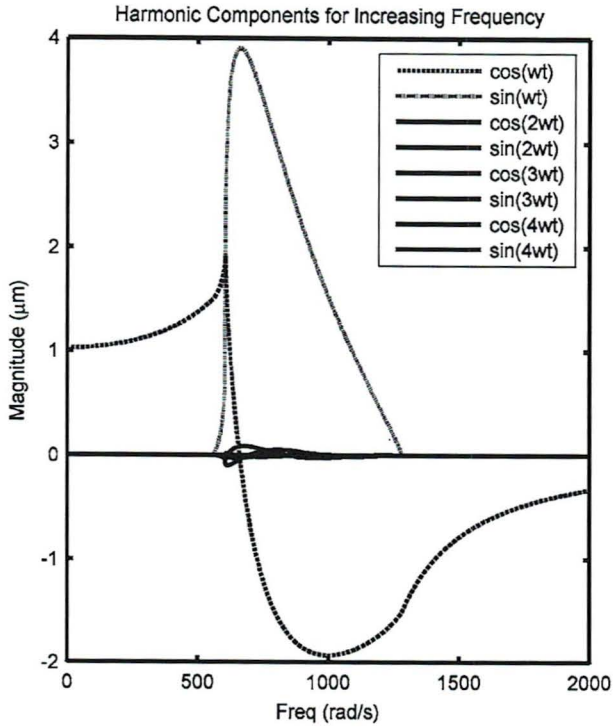

Fig. 7 Typical harmonic components

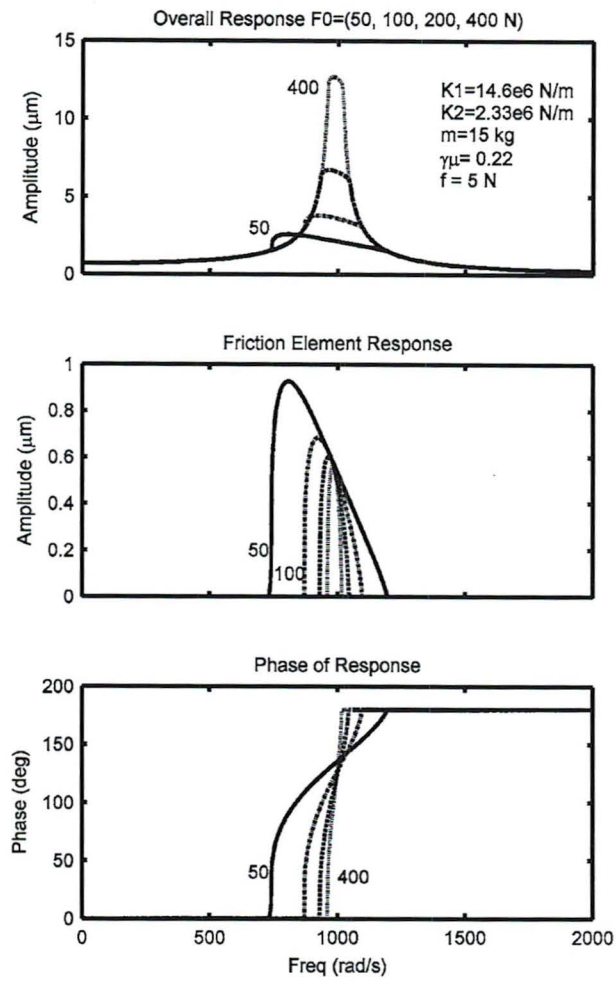

Fig. 8 Effect of static load

tudes provides a significant improvement over simple Coulomb friction, and more nearly reflects foil bearing operational experience.

It is also interesting to note that the general shape of the response is qualitatively similar to several of the coast-down responses presented in [42]. In particular, several of the coast-down responses presented in this reference show a gradual rise in amplitude as speed decreases, followed by a more rapid decrease in amplitude once the rotor passes through the resonance. This matches the general pattern of Fig. 6.

Figure 7 presents the harmonic amplitudes for the MHB solution. As can be seen, the response is primarily synchronous, with some contribution from higher harmonics when the friction element is active. This important result suggests that replacing the nonlinear model with an equivalent stiffness and damping would provide reasonable predictions of the overall dynamic behavior (at least for this case).

Parametric Studies

With some level of confidence in the MHB solution, the next step is to examine a number of parametric studies to evaluate how the various parameters affect the frequency response. These studies consider response versus frequency for:

1. variations in static load,
2. variations in excitation amplitude,
3. variations in friction coefficient, and
4. variations in stiffness ratio.

For each case, three plots will be presented. The first is the peak amplitude versus frequency. The second is the friction element amplitude response. The third is the synchronous phase between excitation and response calculated by combining the cosine and sine components of the response at the excitation frequency into a single complex response, then calculating the phase angle of this response. It should be noted that several of the published experimental data sets correspond to frequency sweeps with a constant excitation amplitude, as opposed to the constant excitation force used for the frequency sweeps presented below.

Parametric Studies 1—Static Load

To evaluate the effect of static load on the model behavior, the total amplitude response versus frequency for four static loads (50, 100, 200, and 400 N) with a nominal dynamic excitation (5 N) was computed using the MHB approach. The results are presented in Fig. 8.

For the case considered, the effective damping decreases as the ratio of static load to dynamic load increases, resulting in increased amplitudes while passing through the resonance. The plot of the friction element response amplitudes suggests that the decrease in damping is probably due to the friction element active region occurring over a narrower frequency band for increased load. This is probably due to the increase in break-away force for the higher static loads. The phase angle plots confirm that the response peaks are resonances, with an approximately 180 deg change. They also agree with the amplitude results that indicate decreasing damping with increasing static to dynamic load ratio for a constant excitation force. As noted previously, most previous work on bump damping has examined response for a constant excitation amplitude. These works indicate increasing damping with increasing static load to dynamic excitation amplitude. As

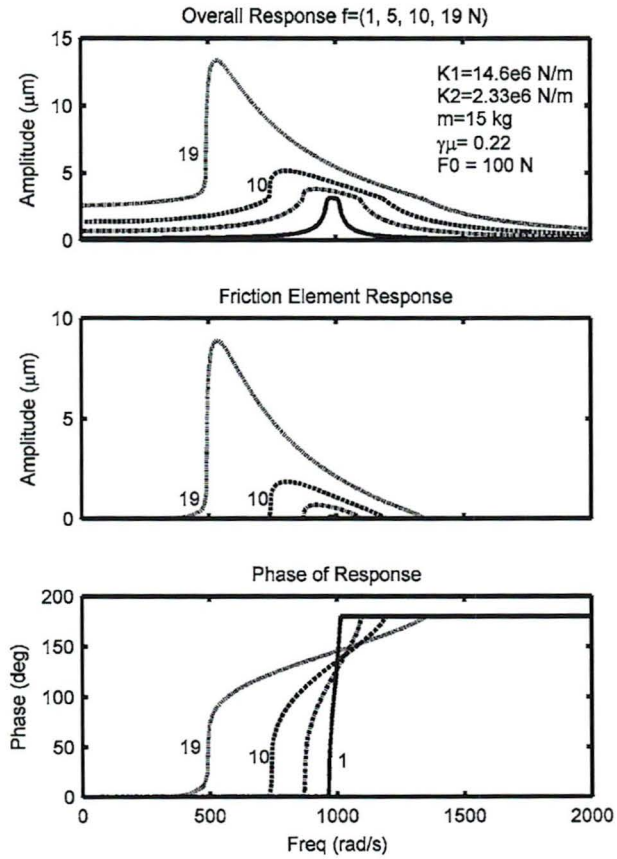

Fig. 9 Excitation amplitude results

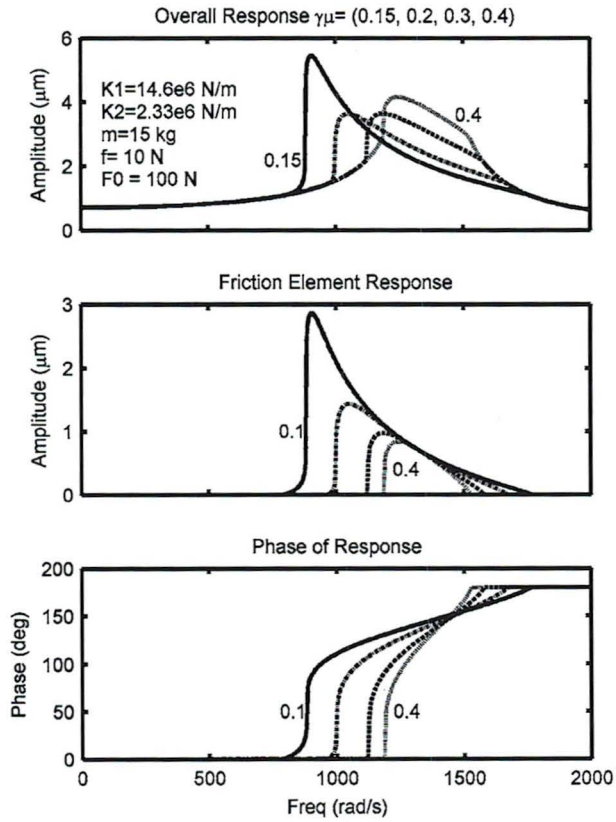

Fig. 10 Effect of changes in friction/coupling coefficient

will be discussed later, the simple bump model does in fact predict this trend when a constant excitation amplitude rather than constant excitation force is considered.

Parametric Studies 2—Excitation Amplitude

To evaluate the effect of dynamic load on the model behavior, the MHB approach is used to calculate the total amplitude response versus frequency for four dynamic excitations (1, 5, 10, and 19 N), with a nominal static load (100 N). The loads range from fairly small to approximately the largest for which the MHB would maintain convergent behavior without amplitudes large enough to cause lift-off (i.e., negative displacements). This was approximately 20% of the applied load in this case over the frequency range considered. The results are presented in Fig. 9.

As with the static load results, the lowest damping occurs for the largest ratio of static to dynamic load. However, in this case, this response also has the smallest overall amplitude. It is interesting to note that for this combination of parameters, the response peak is flattened. For increasing dynamic loads, the overall response increases, as does the friction element amplitude, and the frequency range where the friction element is active. Considering the slope of the phase response at the 90 deg point, damping generally appears to increase as the ratio of dynamic load to static load decreases. The increased amount of friction element motion also appears to provide a softening effect, as evidenced by the decreasing frequency of the resonance.

Parametric Studies 3—Friction/Coupling Coefficient

To evaluate the effect of the friction/coupling coefficient, four coefficients were considered (0.15, 0.2, 0.3, and 0.4) with nominal static and dynamic loads (100 N, 10 N). This friction/coupling coefficient ranged from somewhat less than the one tuned for the flat bump data (0.22) to about twice this value. These results are presented in Fig. 10.

Interestingly, these results tend to suggest an optimum value of the friction/coupling coefficient with regards to minimizing dynamic response. Over the range considered, the largest and smallest values result in larger predicted response amplitudes than the intermediate values. For this parameter set, the tuned value provides one of the smallest responses. This makes some intuitive sense. A very small friction/coupling coefficient would provide very low energy dissipation, and hence low damping. A large coefficient would result in bump locking, which degenerates the model to an undamped spring. The optimum, however, is probably system dependent. The friction element amplitudes and phase responses all change in order of coefficient magnitude.

Parametric Studies 4—Stiffness Ratio

To evaluate the effect of changing the stiffness parameters, three ratios (3, 6, and 12) were considered. These range from approximately half to approximately twice the tuned value. The dynamic excitation was reduced to 5 N to maintain a no-lift-off condition for all three cases. These results are presented in Fig. 11.

These results show a pretty strong and consistent effect of the change in stiffness ratio, with the lowest ratio giving the highest predicted amplitudes. These results tend to suggest that a stiffer connection between the mass and the friction element is better. This conclusion makes sense, as a softer connection reduces the effectiveness of the friction element. Additionally, as the overall system gets stiffer, the resonant frequency increases as would be expected.

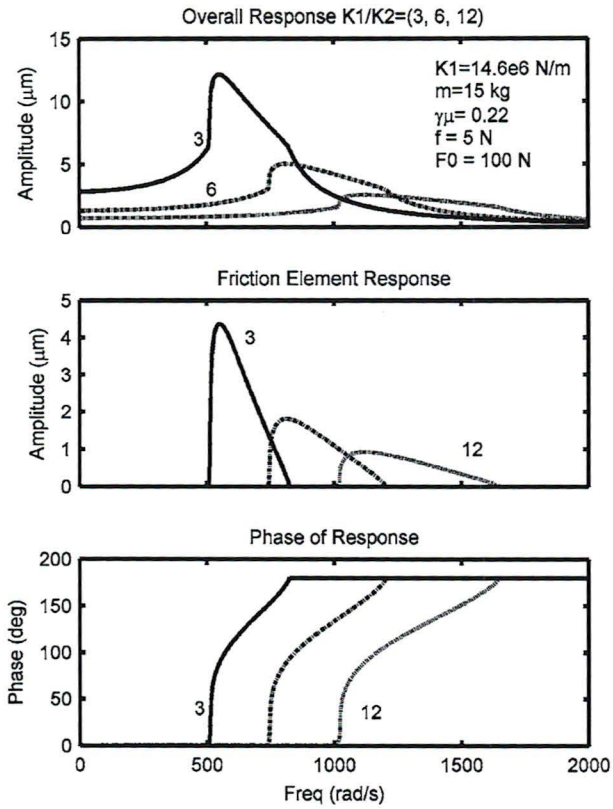

Fig. 11 Effect of stiffness ratio

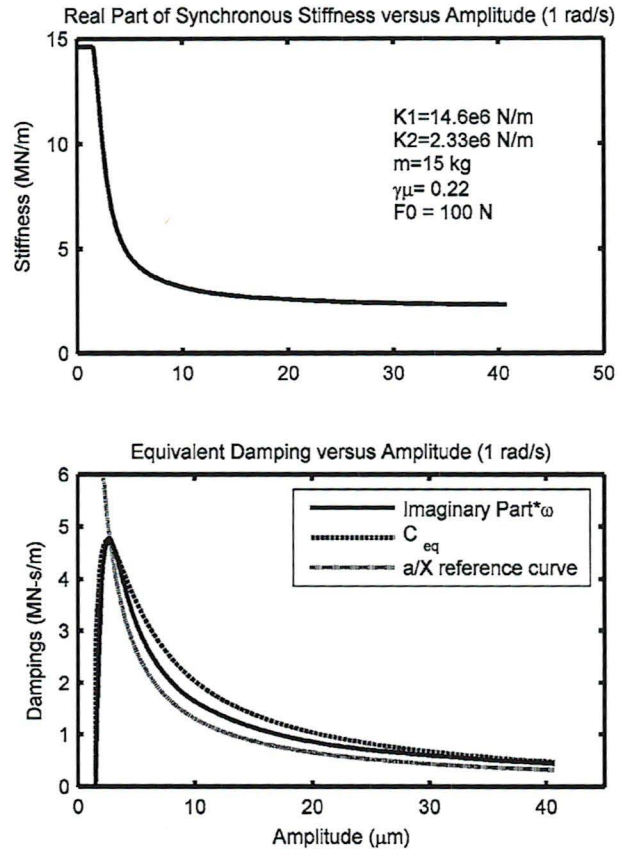

Fig. 12 Equivalent stiffness and damping

Equivalent Stiffness and Damping

Two approaches to examining the equivalent linearized characteristics of the simplified bump model will be presented. The first is numerical using the simple bump-mass system. At an excitation frequency well below resonance, a sweep can be made from static load to a dynamic excitation equal to the static load (i.e., the largest that can be applied without lift-off). The synchronous cosine and sine components can again be combined into complex number, and the ratio of force to complex stiffness can be computed at each sweep frequency. The magnitude of the real part of this ratio is the linear equivalent damping, the magnitude of the imaginary part divided by the excitation frequency is the linear equivalent damping. The results of this calculation for the nominal system are shown in Fig. 12.

A second approach to the prediction of equivalent damping is via the work performed by a simple bump over a cycle [33]. Using the equations for the force versus displacement presented previously, a closed form equation may be developed for the work performed. Some care is necessary, since the average value of the response is a function of both the static load and the dynamic load. After a considerable amount of algebra, the energy-based equivalent damping for conditions where the friction element is moving without lift-off can be expressed as shown in Eq. (10). This equation was evaluated for the nominal system and is as shown in Fig. 12.

$$C_{eq} = 4\frac{\gamma\mu[K1K2(\gamma\mu)^2 + K1^2 + K1K2 - K1^2(\gamma\mu)^2]}{(1-\gamma\mu)(1+\gamma\mu)(K1+K2)^2}\frac{F0}{\pi\omega x} - 4\frac{(\gamma\mu)^2(K1+K2-\gamma\mu K1)}{(1-\gamma\mu)(1+\gamma\mu)(K1+K2)^2}\frac{F0^2}{\pi\omega x^2} - 4\frac{(\gamma\mu)^2K1^2K2}{(1-\gamma\mu)(1+\gamma\mu)(K1+K2)^2}\frac{1}{\pi\omega} \quad (10)$$

The upper plots show that the simple bump model provides a stiffness equal to K_1 until the dynamic load is high enough for the friction element to become active. Once the friction element is active, the equivalent stiffness rapidly approaches a value closer to the series combination of the two springs, as would be expected. This softening characteristic suggests that the behavior of the simple bump model response at resonance is somewhat more complex than a simple linear system in that once the amplitudes grow due to resonant excitation, the system resonance rapidly drops below the excitation frequency.

The equivalent damping is seen to initially increase, rapidly reaching a peak, then decrease. Also shown on the equivalent damping plot is a reference line decreasing at a rate proportional to $1/x$ from the peak equivalent damping. As noted previously, pure Coulomb friction decreases at a rate proportional to $1/x$. This plot shows the simple bump model providing slightly more damping, which helps explain the bounded amplitudes near resonance. Since the simple bump model is a static model (i.e., displacements only), the equivalent damping will decrease proportional to 1/frequency. In this sense, it is similar to a complex stiffness model.

Comparison to Previous Work

The closest published experimental data to a single bump are in the work by Ku [11], which presents dynamic coefficients for 2.5 and 5 μm amplitude, 1 Hz excitation of a flat six bump strip. Comparing the experimental results to the bump model predictions, the simple bump model stiffness and damping predictions are of the same order of magnitude. The experimental results support the general trend of decreasing dynamic stiffness for increasing excitation amplitude as predicted by the simple bump model. The experimental results for damping are less consistent, making

it difficult to draw conclusions. With only two test amplitudes, it is also difficult to compare the model's prediction of a damping peak.

Two other works [26,27] present limited experimental results for a full bearing assembly. The results in [26] show a general decrease in direct stiffness and direct damping with increasing dynamic excitation amplitude. This agrees with the general trends shown in Figs. 9 and 12. The experimental results show a general decrease in direct damping with increasing excitation frequency, which agrees with the previous discussion.

The results in [27] show a roughly linear increase in direct damping with increasing static load, which agrees with Eq. (9). The direct damping again generally decreases with increasing excitation frequency. The results for direct stiffness are somewhat less clear, but do point to a general increase with applied load, which agrees with the trends seen in Fig. 8.

The series of works by Salehi et al. [28,29] provides curve fits that indicate rates of damping decrease of approximately $1/x^{1.2}$ and $1/f^{1.3}$ for partial arc assemblies. These rates are higher than both the model predictions and equivalent Coulomb damping, but do lend some support to the general characteristics predicted by the simple bump model. This work, like most of the previous works, also is based on constant amplitude excitation rather than constant force excitation as in the parametric studies presented previously. These works generally conclude that damping increases as the ratio of static to dynamic load increases. The simple bump model's agreement with this general trend is most clearly shown in the first term of Eq. (10). For the range of coefficients considered, this is the dominant term. Thus, for constant excitation amplitude ("x" in Eq. (10)), the simple bump predicts a roughly linear increase in damping with static load.

Summary, Conclusions and Future Work

This work has presented a preliminary evaluation of a simplified model for bump foil damping. The unique feature of this model is the explicit inclusion of a load-dependent friction element. To develop the model, bump strips with multiple bumps, each with two friction interfaces, are simplified to a single bump with a single friction interface. It is argued that this model predicts behavior that closely resembles the experimental data available for bump foil strips and foil bearings. A number of parametric studies of the behavior of this model are presented. Significantly, they suggest that there may be an optimum level of friction/displacement coupling in a bump foil system for a given bump configuration.

It is argued that the model more nearly meets criteria 1, 3, and 4 for a "good model," as presented in the Introduction, than Coulomb friction. The limit cycle criterion is not examined and is an issue for future work. However, if it is postulated that the root cause of the limit cycles is destabilizing cross-coupled stiffness arising from hydrodynamic effects, it seems likely that the model will predict a limit cycle. The argument would be that the subsynchronous amplitudes must grow to a point where the friction element becomes active, then to a point where the friction element provides adequate damping to dissipate the energy from the cross-coupled force.

Future work to more fully evaluate the usefulness of the model includes careful experimental evaluation of the dynamic characteristics of a single bump, addressing the limit cycle question, as well as attempting to rigorously establish the boundedness of the model near resonance. Additional efforts are also required to integrate this model into a more comprehensive foil bearing analysis.

The very good agreement between the bump strip data, as well as the qualitative similarity to foil bearing responses, suggest the simple, three parameter model is capturing much of the essence of a bump foil's dynamic characteristics. Thus, inclusion of the load dependence of the bump foil friction provides a route to improve bump foil dynamic predictions.

Acknowledgment

The author would like to acknowledge the helpful suggestions and comments on the draft of this paper by Seward W. Pulitzer III.

Nomenclature

- C_{eq} = equivalent linear damping
- F_d = Coulomb friction force
- $F0$ = static force
- F_j^c, F_j^s = force cosine and sine harmonic amplitudes
- K = spring stiffness
- M, m = mass
- $\mathbf{R}$ = frequency domain residual
- $X0$ = static displacement
- X_j^c, X_j^s = displacement cosine and sine harmonic amplitudes
- $\mathbf{Z}$ = frequency domain inertia force matrix
- a = dummy constant of proportionality
- f = generic applied force, applied dynamic force
- i = difference equation time step
- $g(\,)$ = nonlinear force
- x = response amplitude
- x_1 = overall response amplitude
- x_2 = friction element response amplitude
- ω = excitation frequency
- $\gamma\mu$ = friction coefficient multiplied by coupling coefficient

References

[1] Blok, H., and Van Rossum, J. J., 1953, "The Foil Bearing—A New Departure in Hydrodynamic Lubrication," ASME J. Lubr. Technol., **9**, pp. 316–330.

[2] Agrawal, G. L., 1997, "Foil Air/Gas Bearing Technology—An Overview," ASME Paper No. 97-GT-347.

[3] Dellacorte, C., Zaldana, A. R., and Radil, K., 2004, "A Systems Approach to the Solid Lubrication of Foil Air Bearings for Oil-Free Turbomachinery," STLE Tribol. Trans., **126**, pp. 200–207.

[4] Heshmat, H., Walton, J. F., Dellacorte, C., and Valco, M., 2000, "Oil-Free Turbocharger Demonstration Paves Way to Gas Turbine Engine Applications," ASME Paper No. 2000-GT-620.

[5] Swanson, E. E., Heshmat, H., and Shin, J. S., 2002, "The Role of High Performance Foil Bearings in an Advanced, Oil-Free, Integral Permanent Magnet Motor Driven, High-Speed Turbo-Compressor Operating Above the First Bending Critical Speed," ASME Paper No. GT-2002-30579.

[6] DellaCorte, C., and Valco, M. J., 2003, "Oil-Free Turbomachinery Technology for Regional Jet, Rotorcraft and Supersonic Business Jet Propulsion Engines," AIAA Paper No. ISABE-2003-1182.

[7] Oh, K. P., and Rohde, S. M., 1976, "Theoretical Investigation of the Multileaf Journal Bearing," ASME J. Appl. Mech., **43**, pp. 237–242.

[8] Walowit, J. A., Murray, S. F., McCabe, J. T., Arwas, E. B., and Moyer, T., 1973, "Gas Lubricated Foil Bearing Technology Development for Propulsion and Power Systems," Report No. AFAPL-TR-73-92, U.S. Air Force.

[9] Ku, C. P. R., and Heshmat, H., 1992, "Compliant Foil Bearing Structural Stiffness Analysis: Pt 1—Theoretical-Model Including Strip and Variable Bump Foil Geometry," ASME J. Tribol., **114**, pp. 394–400.

[10] Ku, C. P. R., and Heshmat, H., 1994, "Structural Stiffness and Coulomb Damping in Compliant Foil Journal Bearings: Parametric Studies," STLE Tribol. Trans., **37**, pp. 455–462.

[11] Ku, C. P. R., 1994, "Dynamic Structural-Properties of Compliant Foil Thrust-Bearings—Comparison Between Experimental and Theoretical Results," ASME J. Tribol., **116**, pp. 70–75.

[12] Ku, C. P. R., and Heshmat, H., 1994, "Structural Stiffness and Coulomb Damping in Compliant Foil Journal Bearings—Theoretical Considerations," STLE Tribol. Trans., **37**, pp. 525–533.

[13] Heshmat, C. A., Xu, D. S., and Heshmat, H., 2000, "Analysis of Gas Lubricated Foil Thrust Bearings Using Coupled Finite Element and Finite Difference Methods," ASME J. Tribol., **122**, pp. 199–204.

[14] Peng, J.-P., and Carpino, M., 1993, "Calculation of Stiffness and Damping Coefficients for Elastically Supported Gas Foil Bearings," ASME J. Tribol., **115**, pp. 20–27.

[15] Peng, J.-P. and Carpino, M., 1994, "Coulomb Friction Damping Effects in Elastically Supported Gas Foil Bearings," STLE Tribol. Trans., **37**, pp. 91–98.

[16] Peng, J.-P., and Carpino, M., 1997, "Finite Element Approach to the Prediction of Foil Bearing Rotor Dynamic Coefficients," ASME J. Tribol., **119**, pp. 85–90.

[17] Carpino, M., and Talmage, G., 2003, "A Fully Coupled Finite Element Formulation for Elastically Supported Foil Journal Bearings," STLE Tribol. Trans., **46**, pp. 560–565.

[18] Iordanoff, I., Hermal, P., and Stefan, P., 1995, "Optimization of Air Compliant

Thrust Bearings," *Lubricants and Lubrication, Proc. 21th Leeds-Lyon Symposium on Tribology*. D. Dowson, C. M. Taylor, and T. H. C. Childs, eds., September 6–9, Elsevier, Leeds, UK, pp. 283–289.
[19] Iordanoff, I., Hermal, P., and Stefan, P., 1996, "Effect of Compliance on the Extend of Optimum Compliant Air Thrust Bearing Operating Range," *The Third Body Concept, Proc 22nd Leeds/Lyon Symposium on Tribology*. D. Dowson, ed., Lyon, France, September 5–8, Elsevier, Leeds, UK, pp. 453–460.
[20] Iordanoff, I., 1999, "Analysis of an Aerodynamic Compliant Foil Thrust Bearing: Method for a Rapid Design," ASME J. Tribol., **121**, pp. 816–822.
[21] Peng, Z.-C., and Khonsari, M., 2004, "On the Limiting Load-Carrying Capacity of Foil Bearings," ASME J. Tribol., **126**, pp. 817–818.
[22] Peng, Z.-C., and Khonsari, M., 2004, "Hydrodynamic Analysis of Compliant Foil Bearings with Compressible Air Flow," ASME J. Tribol., **126**, pp. 542–546.
[23] San Andres, L., 1995, "Turbulent-Flow Foil Bearings for Cryogenic Applications," ASME J. Tribol., **117**, pp. 185–195.
[24] Kim, T. H., and San Andres, L., 2005, "Heavily Loaded Gas Foil Bearings: A Model Anchored to Test Data," ASME Paper No. GT2005-68486.
[25] Ku, C. P. R., and Heshmat, H., 1993, "Compliant Foil Bearing Structural Stiffness Analysis. 2. Experimental Investigation," ASME J. Tribol., **115**, pp. 364–369.
[26] Heshmat, H., and Ku, C. P. R., 1994, "Structural Damping of Self-Acting Compliant Foil Journal Bearings," ASME J. Tribol., **116**, pp. 76–82.
[27] Ku, C. P. R., and Heshmat, H., 1994, "Effects of Static Load on Dynamic Structural Properties in a Flexible Supported Foil Journal Bearing," ASME J. Vibr. Acoust., **116**, pp. 70–75.
[28] Salehi, M., and Heshmat, H., 2002, "Frictional Dampers Dynamic Characterization—Theory and Experiments," *Boundary and Mixed Lubrication: Science and Applications, Proceedings of the 28th Leeds-Lyon Symposium on Tribology*. D. Dowson, M. Priest, and G. Dalmaz, eds., Amsterdam, Netherlands, September 4–7, Elsevier, Leeds, UK, pp. 515–526.
[29] Salehi, M., Heshmat, H., and Walton, J. F., 2003, "On the Frictional Damping Characterization of Compliant Bump Foils," ASME J. Tribol., **125**, pp. 804–813.
[30] Rubio, D., and Andres, L. S., 2004, "Bump-Type Foil Bearing Structural Stiffness: Experiments and Predictions," ASME Paper No. GT2005-68486.
[31] Salehi, M., Heshmat, H., and Walton, J. F. III, 2004, "Advancements in the Structural Stiffness and Damping of a Large Compliant Foil Journal Bearing: An Experimental Study," ASME Paper No. GT2004-53860.
[32] Rubio, D., and San Andres, L., 2005, "Structural Stiffness, Dry-Friction Coefficient and Equivalent Viscous Damping in a Bump-Type Foil Gas Bearing," ASME Paper No. GT2005-68384.
[33] Thomson, W. T., 1988, *Theory of Vibration with Applications*, Prentice Hall, Englewood Cliffs, NJ.
[34] Whiteman, W. E., and Ferri, A. A., 1996, "Displacement-Dependent Dry Friction Damping of a Beam-Like Structure," J. Sound Vib., **198**, pp. 313–329.
[35] Menq, C.-H., Griffin, J. H., and Bielak, J., 1986, "The Influence of a Variable Normal Load on the Forced Vibration of a Frictionally Damped Structure," ASME J. Eng. Gas Turbines Power, **108**, pp. 300–305.
[36] Swevers, J., Al-Bender, F., Ganseman, C. G., and Prajogo, T., 2000, "Integrated Friction Model Structure with Improved Presliding Behavior for Accurate Friction Compensation," IEEE Trans. Autom. Control, **45**, pp. 675–686.
[37] Lampaert, V., Swevers, J., and Al-Bender, F., 2002, "Modification of the Leuven Integrated Friction Model Structure," IEEE Trans. Autom. Control, **47**, pp. 683–687.
[38] Lampaert, V., Al-Bender, F., and Swevers, J., 2003, "A Generalized Maxwell-Slip Friction Model Appropriate for Control Purposes," *Proceedings of the IEEE Intl. Conf. on Physics and Control*, St. Petersburg, Russia, August 20–22.
[39] Narayanan, S., and Sekar, P., 1994, "Bifurcation and Chaos of Coupled Systems by Fast Incremental Harmonic Balancing," *Nonlinearity and Chaos in Engineering Dynamics*. J. M. T. Thompson and S. R. Bishop, eds., John Wiley, New York, pp. 365–375.
[40] Petrov, E. P., 2004, "Method for Direct Parametric Analysis of Nonlinear Forced Response of Bladed Discs with Friction Contact Interfaces," ASME J. Turbomach., **126**, pp. 654–662.
[41] Mathworks, 2005, *Optimization Toolbox for Use with Matlab: User's Guide*, Mathworks, Natick, MA.
[42] Walton, J. F. II, and Heshmat, H., 2002, "Application of Foil Bearings to Turbomachinery Including Vertical Operation," ASME J. Eng. Gas Turbines Power, **124**, pp. 1032–1041.